*Inorg. Chem.* **2008**, *47*, 9471−9477

# Polygallide $RE_2MGa_9Ge_2$ (RE = Ce, Sm; M = Ni, Co) Phases Grown in Molten Gallium

**Marina A. Zhuravleva and Mercouri G. Kanatzidis***

*Department of Chemistry, Northwestern University, Evanston, Illinois 60208*

Received June 10, 2008

The quaternary intermetallics $Ce_2CoGa_9Ge_2$, $Ce_2NiGa_9Ge_2$, and $Sm_2NiGa_9Ge_2$ were prepared by reacting elemental metals in excess of gallium at 850 °C. The title compounds crystallize in the tetragonal space group *P*4/*nmm* in the $Sm_2Ni(Si_{1-x}Ni_x)Al_4Si_6$ structure type with cell parameters $a = 5.9582(5)$ Å, $c = 15.0137(18)$ Å, and $a = 5.9082(17)$ Å, $c = 14.919(6)$ Å, $Z = 2$, for $Ce_2CoGa_9Ge_2$ and $Sm_2NiGa_9Ge_2$, respectively. The structures are composed of covalently bonded three-dimensional networks of $[CoGa_9Ge_2]$ in which the rare-earth metals fill the voids forming a 2D square net. The structures of $RE_2MGa_9Ge_2$ are Ga-rich and possess extensive Ga−Ga bonding even though the Ga atoms do not form a network on their own. Magnetic susceptibility measurements for $Ce_2CoGa_9Ge_2$ and $Ce_2NiGa_9Ge_2$ show Curie−Weiss paramagnetism, consistent with presence of $Ce^{3+}$ ions. Magnetocrystalline anisotropy was observed for $Ce_2NiGa_9Ge_2$, with the magnetically easy axis lying along the [001] crystallographic direction. A transition to an antiferromagnetic state was observed below 4 K in the easy direction of magnetization. In the magnetically hard direction of the basal plane, paramagnetic behavior was observed down to 1.8 K.

## Introduction

Complex gallium-containing intermetallics have shown fascinating physical properties such as superconductivity in $PuCoGa_5$,[1−3] magnetoresistance in $SmPd_2Ga_2$,[4] and heavy fermion behavior in $CePdGa_6$.[5] A large number of binary and ternary intermetallics have been reported;[6−13] however, quaternary systems have not been investigated in detail. The application of the metal flux technique to the synthesis of complex intermetallics, including rare-earth (RE), transition metal (M), and the main group 13 and 14 elements such as Ga, Al, In, and Si, Ge, had so far shown exceptional results.[14] In investigations using molten Ga as a solvent, we have already described the systems with M = Fe, Ni, and Co. In the case of Fe, $Tb_4FeGe_8$[15] and the gallide $RE_4FeGa_{12-x}Ge_x$[16] have been discovered to form when RE/Fe > 1 in the reaction. For the systems with M = Ni and Co, we thus far mostly examined the cases with the RE/M ≤ 1. From these reactions, several ternary and quaternary intermetallic compounds have been synthesized. Examples include $RENiSi_3$,[17]

* To whom correspondence should be addressed. E-mail: m-kanatzidis@northwestern.edu.

(1) Sarrao, J. L.; Morales, L. A.; Thompson, J. D.; Scott, B. L.; Stewart, G. R.; Wastin, F.; Rebizant, J.; Boulet, P.; Colineau, E.; Lander, G. H. *Nature* **2002**, *420* (6913), 297–299.
(2) Curro, N. J.; Caldwell, T.; Bauer, E. D.; Morales, L. A.; Graf, M. J.; Bang, Y.; Balatsky, A. V.; Thompson, J. D.; Sarrao, J. L. *Nature* **2005**, *434* (7033), 622–625.
(3) Opahle, I.; Oppeneer, P. M. *Phys. Rev. Lett.* **2003**, (15), 90.
(4) Williams, W. M.; Macaluso, R. T.; Moldovan, M.; Young, D. P.; Chan, J. Y. *Inorg. Chem.* **2003**, *42* (22), 7315–7318.
(5) Macaluso, R. T.; Millican, J. N.; Nakatsuji, S.; Lee, H. O.; Carter, B.; Moreno, N. O.; Fisk, Z.; Chan, J. Y. *J. Solid State Chem.* **2005**, *178* (11), 3547–3553.
(6) Sichevych, O.; Schnelle, W.; Prots, Y.; Burkhardt, U.; Grin, Y. *Z. Naturforsch., B: Chem. Sci.* **2006**, *61* (7), 904–911.
(7) Bostrom, M.; Prots, Y.; Grin, Y. *J. Solid State Chem.* **2006**, *179* (8), 2472–2478.
(8) Vasylechko, L.; Schnelle, W.; Schmidt, M.; Burkhardt, U.; Borrmann, H.; Schwarz, U.; Grin, Y. *J. Alloys Compd.* **2006**, *416* (1−2), 35–42.
(9) Fedorchuk, A.; Prots, Y.; Grin, Y. *Z. Kristallogr.- New Cryst. Struct.* **2005**, *220* (3), 317–318.
(10) Vasylechko, L.; Schnelle, W.; Burkhardt, U.; Ramlau, R.; Niewa, R.; Borrmann, H.; Hiebl, K.; Hu, Z.; Grin, Y. *J. Alloys Compd.* **2003**, *350* (1−2), 9–16.
(11) Giedigkeit, R.; Niewa, R.; Schnelle, W.; Grin, Y.; Kniep, R. *Z. Anorg. Allg. Chem.* **2002**, *628* (7), 1692–1696.
(12) Grin, Y.; Ellner, M.; Predel, B.; Baumgartner, B. *J. Solid State Chem.* **1995**, *114* (2), 342–345.
(13) Jardin, R.; Colineau, E.; Wastin, F.; Rebizant, J.; Sanchez, J. P. *Physica B* **2006**, *378−80*, 1031–1032.
(14) Kanatzidis, M. G.; Pottgen, R.; Jeitschko, W. *Angew. Chem., Int. Ed.* **2005**, *44* (43), 6996–7023.
(15) Zhuravleva, M. A.; Bilc, D.; Pcionek, R. J.; Mahanti, S. D.; Kanatzidis, M. G. *Inorg. Chem.* **2005**, *44* (7), 2177–2188.
(16) Zhuravleva, M. A.; Wang, X. P.; Schultz, A. J.; Bakas, T.; Kanatzidis, M. G. *Inorg. Chem.* **2002**, *41* (23), 6056–6061.
(17) Chen, X. Z.; Larson, P.; Sportouch, S.; Brazis, P.; Mahanti, S. D.; Kannewurf, C. R.; Kanatzidis, M. G. *Chem. Mater.* **1999**, *11* (1), 75–83.

10.1021/ic801067g CCC: $40.75 
Published on Web 09/24/2008

$RE_2Ni_{3+x}Si_{5-x}$,[18] $RE_{0.67}M_2Ga_{5-x}Ge_x$,[19] $RE_{0.67}M_2Ga_{6-x}Ge_x$,[19] $REMGa_3Ge$,[20] $RE_3Ni_3Ga_8Ge_3$,[20] and $GdCo_{1-x}Ga_3Ge$.[21] Although in the Si-containing system RE/Ni/Ga/Si the compositions with RE/Ni > 1 were previously studied, systematic investigations in the related RE/M/Ga/Ge system have not yet been performed.

Herein we present the results of the exploratory synthesis in the RE/M/Ga/Ge system with RE/M > 1 (M = Ni and Co) employing molten Ga as a solvent. We describe the synthesis, structure, and magnetic properties of three novel intermetallics $Ce_2CoGa_9Ge_2$, $Ce_2NiGa_9Ge_2$, and $Sm_2NiGa_9Ge_2$. Fascinatingly, we find that these reactions yield predominantly quaternary compounds, whereas in the analogous reactions in RE/Ni/Ga/Si system mostly gave ternary $RE_5Co_4Si_{14}$,[22] $RENiSi_3$,[17] $RE_2NiGa_{12}$[23] and pseudoternary $RE_2NiGa_{12-x}Si_x$ intermetallic compounds. The dichotomy in reaction chemistry of RE/M/Ga/Ge and RE/M/Ga/Si systems is discussed.

## Experimental Methods

**Synthesis.** Elemental Ce, Sm (2.26 mmol), Co, Ni (1.13 mmol), and Ge (3.4 mmol) of typical purity 99.9% and higher (CERAC Inc.) were combined in the molar ratio 2:1:3 with 30 equiv of Ga (33 mmol) and placed in the alumina crucibles. The metals were handled in the dry box under nitrogen atmosphere. The crucibles were then sealed in the quartz ampule under high vacuum ($\sim 1 \times 10^{-4}$ Torr). The reaction mixtures were heated to 1000 °C in 15 h, left at 1000 °C for 5 h to allow proper homogenization of the melt, cooled in 2 h to 850 °C, kept there isothermally for 6 days, and cooled to 250 °C at the rate of 8°/h. Unreacted Ga flux was removed by hot-filtration at 250 °C via centrifuging through a specially designed quartz filter with a coarse frit. Further isolation was done in 3−5 molar solution of iodine in dimethylformamide (DMF) over 12−24 h at room temperature. The product was rinsed with hot water and DMF and dried with acetone and ether. The crystals of $RE_2MGa_9Ge_2$ are large, plate-like, often displaying a phyllomorphous character. High yield (>90%) of the $Ce_2CoGa_9Ge_2$ and $Ce_2NiGa_9Ge_2$ phases was observed under the described conditions. However, they appear to be suboptimal for the synthesis of $Sm_2NiGa_9Ge_2$ under which a mixture of $Sm_3Ni_3Ga_8Ge_3$ and $Sm_2NiGa_9Ge_2$ phases was produced in approximately 2:3 molar ratio. The yield of $Sm_2NiGa_9Ge_2$ is enhanced to ~80% (from ~30%) by limiting the heating time to only 5 h at 1000 °C. The side products of this reaction are $Sm_3Ga_9Ge$[24] and recrystallized Ge.

**Elemental Analysis and X-ray Powder Diffraction.** The purity and the identity of the products were confirmed by elemental analysis and X-ray powder diffraction (XRD). Semiquantitative microprobe elemental analysis was performed using a scanning electron microscope equipped with the NORAN energy dispersive spectrometer. The routine data acquisition was done at an acceleration voltage of 20 kV and a collection time of 30 s. An extensive averaging of the results obtained on the different crystals was carried out to attain accurate values of the atomic ratios. Averaged compositions for $Ce_2CoGa_9Ge_2$ were determined to be "$Ce_2Co_{1.3}Ga_{6.1}Ge_{4.0}$" (normalized to the amount of Ce). Similar results were obtained for the Sm/Ni/Ga/Ge and Ce/Ni/Ga/Ge compounds. The XRD patterns of products were taken at room temperature on a CPS 120 INEL X-ray diffractometer (Cu Kα radiation) equipped with position-sensitive detector. Experimental XRD patterns were then compared to that calculated from single crystal data using the CERIUS[2] software package.[25]

**Single Crystal X-ray Crystallography.** The intensity data was collected on single crystals of $Ce_2CoGa_9Ge_2$ and $Sm_2NiGa_9Ge_2$ with a Siemens Platform SMART[26] CCD X-ray diffractometer. A full sphere of reciprocal data (Mo Kα radiation, $\lambda = 0.71073$ Å) was acquired up to 46° in $2\theta$ using $\omega$-steps of 0.30° and an exposure time of 40−50 s per frame. The data collection and acquisition was performed with the SMART[26] software package; the SAINT-PLUS[27] program was used for data reduction. The analytical absorption corrections were done using a face-indexing routine, and an empirical correction for absorption based on symmetry equivalent reflections was consequently applied with the SADABS[28] software package. The crystal structure was solved with direct methods using the SHELXTL[29] program. All atomic positions were refined anisotropically. The setting of the cell was standardized with the STRUCTURE TIDY program.[30]

The $Ce_2CoGa_9Ge_2$ and $Sm_2NiGa_9Ge_2$ crystallize in tetragonal space group *P4/nmm* in a structure type of $Sm_2Ni(Si_{1-x}Ni_x)Al_4Si_6$.[31] In the structure of $RE_2MGa_9Ge_2$, a total of seven atomic positions were identified; of those, sites with multiplicity *4f* and *2a* were unambiguously assigned to rare-earth and transition metal atoms, respectively. Contrarily to the $Sm_2Ni(Si_{1-x}Ni_x)Al_4Si_6$, the substitution of Ge at *2c* with a transition metal was not favorable during the structure refinement of $RE_2MGa_9Ge_2$. The variation of the Ga/Ge versus Al/Si assignment further underlies the differences in $RE_2MGa_9Ge_2$ and its structure type. The accurate determination of the Ga and Ge distribution is very difficult if relying on X-ray diffraction data solely. Here, the assignment of Ga (*8j*, *2c*, *2c*) and Ge (*2c*, *2c*) was made on the basis of elemental analysis, bond length, and connectivity data. Because Ge has a smaller covalent radius than Ga, the shorter Ce−X distances (where X could be Ga or Ge) were assigned to Ge. Previous Ga/Ge and Al/Si assignments based on this approach were shown to be accurate and later confirmed with neutron single crystal diffraction data.[32,33] Further investigation of the Ga/Ge distribution has to be carried out with neutron diffraction or X-ray diffraction with anomalous scattering. The information relevant to the data collection structure refinement, the final atomic positions, and the equivalent thermal displacement


(18) Zhuravleva, M. A.; Kanatzidis, M. G. *Z. Naturforsch., B: Chem. Sci.* **2003**, *58* (7), 649–657.
(19) Zhuravleva, M. A.; Chen, X. Z.; Wang, X. P.; Schultz, A. J.; Ireland, J.; Kannewurf, C. K.; Kanatzidis, M. G. *Chem. Mater.* **2002**, *14* (7), 3066–3081.
(20) Zhuravleva, M. A.; Pcionek, R. J.; Wang, X. P.; Schultz, A. J.; Kanatzidis, M. G. *Inorg. Chem.* **2003**, *42* (20), 6412–6424.
(21) Zhuravleva, M. A.; Evain, M.; Petricek, V.; Kanatzidis, M. G. *J. Am. Chem. Soc.* **2007**, *129* (11), 308.
(22) Salvador, J. R.; Malliakas, C.; Gour, J. R.; Kanatzidis, M. G. *Chem. Mater.* **2005**, *17* (7), 1636–1645.
(23) Chen, X. Z.; Small, P.; Sportouch, S.; Zhuravleva, M.; Brazis, P.; Kannewurf, C. R.; Kanatzidis, M. G. *Chem. Mater.* **2000**, *12* (9), 2520–2522.
(24) Zhuravleva, M. A.; Kanatzidis, M. G. *J. Solid State Chem.* **2003**, *173* (2), 280–292.
(25) *CERIUS*, Version 1.6; Molecular Simulations Inc.: Cambridge, U.K., 1994.
(26) *SMART*, Version 5; Siemens Analytical X-ray Systems, Inc.: Madison, WI, 1998.
(27) *SAINT*, Version 4; Siemens Analytical X-ray Systems, Inc.: Madison, WI, 1994− 1996.
(28) Sheldrick, G. M., *SADABS*; University of Göttingen: Göttingen, Germany.
(29) Sheldrick, G. M. *SHELXTL*, Version 5.1; Siemens Analytical X-ray Systems, Inc.: Madison, WI, 1997.
(30) Gelato, L. M.; Parthe, E. *J. Appl. Crystallogr.* **1987**, *20*, 139–143.
(31) Chen, X. Z.; Sportouch, S.; Sieve, B.; Brazis, P.; Kannewurf, C. R.; Cowen, J. A.; Patschke, R.; Kanatzidis, M. G. *Chem. Mater.* **1998**, *10* (10), 3202–3211.

**Table 1.** Crystal Data and Structure Refinement for (a) $Ce_2CoGa_9Ge_2$ and (b) $Sm_2NiGa_9Ge_2$

| empirical formula | (a) $Ce_2CoGa_9Ge_2$ | (b) $Sm_2NiGa_9Ge_2$ |
|---|---|---|
| formula weight | 1111.83 | 1132.07 |
| temperature (K) | 173(2) | 298(2) |
| wavelength (Å) | 0.71073 | 0.71073 Å |
| crystal system | tetragonal | tetragonal |
| space group | *P4/nmm* | *P4/nmm* |
| unit cell dimensions (Å) | $a = 5.9582(5)$ | $a = 5.9082(17)$ |
| | $c = 15.0137(18)$ | $c = 14.919(6)$ |
| volume (Å$^3$) | 532.99(9) | 520.8(3) |
| $Z$ | 2 | 2 |
| density (calculated) (g/cm$^3$) | 6.928 | 7.220 |
| absorption coefficient (mm$^{-1}$) | 37.663 | 41.297 |
| $F$(000) | 972 | 990 |
| crystal size (mm$^3$) | 0.02 × 0.06 × 0.10 | 0.20 × 0.16 × 0.04 |
| $\theta$ range for data collection | 2.71 to 23.23° | 1.36 to 23.13° |
| index ranges | $-6 \le h \le 6$, $-6 \le k \le 6$, $-16 \le l \le 16$ | $-4 \le h \le 6$, $-4 \le k \le 6$, $-16 \le l \le 13$ |
| reflections collected | 3197 | 1946 |
| independent reflections | 270 [$R_{int} = 0.0338$] | 267 [$R_{int} = 0.0593$] |
| completeness to $\theta$ | 99.6% | 100.0% |
| refinement method | full-matrix least-squares on $F^2$ | |
| data/restraints/parameters | 270/0/29 | 267/0/29 |
| goodness-of-fit on $F^2$ | 1.426 | 1.417 |
| final $R$ indices [$I > 2\sigma(I)$][a] | $R_1 = 0.0194$, $wR_2 = 0.0506$ | $R_1 = 0.0396$, $wR_2 = 0.1304$ |
| $R$ indices (all data) | $R_1 = 0.0221$, $wR_2 = 0.0514$ | $R_1 = 0.0405$, $wR_2 = 0.1308$ |
| extinction coefficient | 0.00243(16) | 0.0020(4) |
| largest diff. peak and hole (e Å$^{-3}$) | 0.630 and −0.996 | 1.978 and −1.897 |

[a] $R_1 = \sum||F_o| - |F_c||/\sum|F_o|$; $wR_2 = [\sum w(|F_o| - |F_c|)^2/\sum w|F_o|^2]^{1/2}$, $w = 1/\sigma^2\{|F_o|\}$.

**Table 2.** Atomic Coordinates and Equivalent Isotropic Displacement Parameters (×10$^3$ Å$^2$) for $Ce_2CoGa_9Ge_2$ (First Row) $Sm_2NiGa_9Ge_2$ (Second Row)

| atomic position | Wyckoff symbol | $x$ | $y$ | $z$ | $U$(eq)[a] |
|---|---|---|---|---|---|
| Ce | *4f* | 3/4 | 1/4 | 0.2529(1) | 6(1) |
| Sm | *4f* | 3/4 | 1/4 | 0.2548(1) | 2(1) |
| Co | *2a* | 3/4 | 1/4 | 0 | 6(1) |
| Ni | *2a* | 3/4 | 1/4 | 0 | 3(1) |
| Ga(1) | *8j* | 0.0103(1) | 0.0103(1) | 0.0851(1) | 7(1) |
| | *8j* | 0.0110(3) | 0.0110(3) | 0.0877(2) | 4(1) |
| Ga(2) | *8j* | 0.0362(2) | 0.0362(2) | 0.4190(1) | 9(1) |
| | *8j* | 0.0333(4) | 0.0333(4) | 0.4179(2) | 8(1) |
| Ga(3) | *2c* | 1/4 | 1/4 | 0.6471(2) | 8(1) |
| | *2c* | 1/4 | 1/4 | 0.6513(3) | 6(1) |
| Ge(1) | *2c* | 1/4 | 1/4 | 0.8130(2) | 8(1) |
| | *2c* | 1/4 | 1/4 | 0.8157(3) | 6(1) |
| Ge(2) | *2c* | 1/4 | 1/4 | 0.2115(2) | 7(1) |
| | *2c* | 1/4 | 1/4 | 0.2151(4) | 7(1) |

[a] $U$(eq) is defined as one-third of the trace of the orthogonalized $U^{ij}$ tensor.

parameters are given in the Tables 1 and 2, respectively. Selected interatomic distances (up to 3.5 Å) and anisotropic displacement parameters refined for $Ce_2CoGa_9Ge_2$ are listed in Tables 3 and 4, respectively. The bond angles are given in the Supporting Information.

**Magnetic Measurements.** The magnetic susceptibilities were measured on single crystal and polycrystalline samples of $Ce_2NiGa_9Ge_2$, and $Ce_2CoGa_9Ge_2$ in the temperature range 1.8−400 K using a MPMS SQUID magnetometer (Quantum Design, Inc.) with the magnetic field 500 Gauss. *Sample preparation:* the crystals were picked manually and polished with sandpaper (600−1500 grit) to eliminate the risk of contamination with unreacted Ni, Co, or Ni-, Co-containing phases. As-obtained samples were further treated with 30% (v/v) solution of HCl for approximately 1 min under sonication, then rinsed with water, and dried with acetone and ether. The anisotropic measurements were performed using single crystal samples by positioning them with the *c*-axis parallel and perpendicular to the external magnetic field ($H_{ex}$). For isotropic measurements, polycrystalline samples were used. The field dependence of magnetization was studied at 2−3 K in fields up to ±5 T. The susceptibility data was corrected for the sample holder contribution.

## Results and Discussion

**Reaction Chemistry.** In employing Ga flux as a synthetic medium for the exploratory synthesis in the RE/M/Ga/Ge system with M = Ni, Co, we find that the formation of the quaternary phases is extremely favorable. To date, we have discovered six families of quaternary compounds: $RE_2MGa_9Ge_2$, $REMGa_3Ge$,[20] $RE_3Ni_3Ga_8Ge_3$,[20] $RE_4Ni_3Ga_6Ge_4$,[20] $RE_{0.67}M_2Ga_{5-x}Ge_x$, and $RE_{0.67}M_2Ga_{6-x}Ge_x$.[19,21] This is unlike the chemistry of the related RE/M/Ga/Si or RE/M/In/Ge systems, where the flux metal tends to act as an unreactive solvent to produce ternary phases such as $RE_5Co_4Si_{14}$,[22] $RENiSi_3$,[17] $RE_2Ni_{3+x}Si_{5-x}$,[18] $YbNi_2Ge_2$,[34] $\beta$-$RENiGe_2$,[35] and $RE_2Zn_3Ge_6$.[36] By contrast, switching from Ga flux to Al flux in Si and Ge containing systems, we again observe the quaternary phases $Sm_2Ni(Si_{1-x},Ni_x)Al_4Si_6$,[31] $RENiAl_4Ge_2$ (RE = Sm, Tb, Y),[37] $RE_4Fe_{2+x}Al_{7-x}Si_8$ (RE = Ce, Pr, Nd, Sm),[38] $RE_8Ru_{12}Al_{49}Si_9[Al_xSi_{12-x}]$ (RE = Sm and Pr),[33]

(32) Chen, X. Z.; Sieve, B.; Henning, R.; Schultz, A. J.; Brazis, P.; Kannewurf, C. R.; Cowen, J. A.; Crosby, R.; Kanatzidis, M. G. *Angew. Chem., Int. Ed.* **1999**, *38* (5), 693–696.
(33) Sieve, B.; Chen, X. Z.; Henning, R.; Brazis, P.; Kannewurf, C. R.; Cowen, J. A.; Schultz, A. J.; Kanatzidis, M. G. *J. Am. Chem. Soc.* **2001**, *123* (29), 7040–7047.
(34) Bud'ko, S. L.; Islam, Z.; Wiener, T. A.; Fisher, I. R.; Lacerda, A. H.; Canfield, P. C. *J. Magn. Magn. Mater.* **1999**, *205* (1), 53–78.
(35) Salvador, J. R.; Gour, J. R.; Bilc, D.; Mahanti, S. D.; Kanatzidis, M. G. *Inorg. Chem.* **2004**, *43* (4), 1403–1410.
(36) Salvador, J. R.; Bilc, D.; Gour, J. R.; Mahanti, S. D.; Kanatzidis, M. G. *Inorg. Chem.* **2005**, *44* (24), 8670–8679.
(37) Sieve, B.; Chen, X.; Cowen, J.; Larson, P.; Mahanti, S. D.; Kanatzidis, M. G. *Chem. Mater.* **1999**, *11* (9), 2451–2455.
(38) Sieve, B.; Sportouch, S.; Chen, X. Z.; Cowen, J. A.; Brazis, P.; Kannewurf, C. R.; Papaefthymiou, V.; Kanatzidis, M. G. *Chem. Mater.* **2001**, *13* (2), 273–283.

**Table 3.** Selected Bond Lengths [Å] for $Ce_2CoGa_9Ge_2$

| bond | distance | multiplicity | bond | distance | multiplicity |
|---|---|---|---|---|---|
| Ce−Ge(2) | 3.0430(6) | × 2 | Ga(1)−Ge(1) | 2.6743(18) | × 1 |
| Ce−Ge(1) | 3.1387(8) | × 2 | Ga(1)−Ge(2) | 2.772(2) | × 1 |
| Ce−Ga(2) | 3.2789(11) | × 4 | Ga(1)−Ga(1) | 2.8566(17) | × 2 |
| Ce−Ga(1) | 3.2843(11) | × 4 | Ga(2)−Ga(2) | 2.508(2) | × 1 |
| Ce−Ga(3) | 3.3362(12) | × 2 | Ga(2)−Ga(2) | 2.5482(18) | × 2 |
| Co−Ga(1) | 2.4655(6) | × 8 | Ga(2)−Ga(3) | 2.6075(16) | × 1 |
| Ga(1)−Ga(1) | 2.562(2) | × 1 | Ga(3)−Ge(1) | 2.490(3) | × 1 |

**Table 4.** Anisotropic Displacement Parameters ($\times 10^3$ Å$^2$) for $Ce_2CoGa_9Ge_2$ (**1**)[a]

| Atomic Position | U11 | U22 | U33 | U23 | U13 | U12 |
|---|---|---|---|---|---|---|
| Ce | 4(1) | 4(1) | 8(1) | 0 | 0 | 0 |
| Co | 4(1) | 4(1) | 8(1) | 0 | 0 | 0 |
| Ga(1) | 6(1) | 6(1) | 9(1) | 0(1) | 0(1) | 1(1) |
| Ga(2) | 7(1) | 7(1) | 12(1) | −2(1) | −2(1) | −1(1) |
| Ga(3) | 7(1) | 7(1) | 10(1) | 0 | 0 | 0 |
| Ge(1) | 7(1) | 7(1) | 10(1) | 0 | 0 | 0 |
| Ge(2) | 6(1) | 6(1) | 10(1) | 0 | 0 | 0 |

[a] The anisotropic displacement factor exponent takes the form: $-2\pi^2[h^2a^2U^{11} + ... + 2hkabU^{12}]$.

$Tb_2NiAl_4Ge_2$,[39] and $Ce_2NiAl_{6-x}Ge_{4-y}$.[39] Such a disparity in Si versus Ge chemistry is perplexing, given their similar covalent bond radii and isoelectronic nature. The higher affinity of Ga toward Ge rather than Si appears to be fine-tuned; understanding the fundamentals underlying these differences will require further investigations.

The ability to grow Ga-free ternary silicides from the RE/M/Ga/Si melts does not seem to depend on the RE/M ratio. For the systems containing Ge, however, the RE/M ratio becomes an important factor in phase formation. For instance, at RE/M < 1, two families of hexagonal phases $RE_{0.67}M_2Ga_{5-x}Ge_x$ and $RE_{0.67}M_2Ga_{6-x}Ge_x$[19] form with nearly every rare-earth: Y, Sm, Gd, Tb, Dy, Ho, Er, Tm, and Yb. At RE/M ≥ 1, however, the products appear to be sensitive to the reaction conditions (temperature, time) and vary with the identity of the rare-earth. For example, the growth of the $RE_2MGa_9Ge_2$ phase was observed only with the lighter lanthanides such as Ce and Sm, while for the heavier rare-earths other structures including $REMGa_3Ge$,[20] $GdCo_{1-x}Ga_3Ge$,[21] and $RE_3Ni_3Ga_8Ge_3$[20] are favored. The chemistry of the Sm/Ni/Ga/Ge system is particularly complex. Up to three quaternary phases $SmNiGa_3Ge$, $Sm_3Ni_3Ga_8Ge_3$,[20] $Sm_2NiGa_9Ge_2$, and a ternary $Sm_3Ga_9Ge$[24] could be found depending on the annealing time and/or the reaction mixture composition. For instance, $Sm_2NiGa_9Ge_2$ seems to be a kinetic product, forming on the early stages of the reaction. $Sm_3Ni_3Ga_8Ge_3$ phase, on the other hand, emerges upon further heating of the reaction mixture, indicative of a thermodynamic stability of this product. Coincidentally, the separation of these two phases was possible owing to the variation in adhesive properties of these two compounds. Thus, during high-temperature filtration using glass wool as a filter, the crystals of $Sm_3Ni_3Ga_8Ge_3$ phase were found at the filter, while crystals of $Sm_2NiGa_9Ge_2$ settled down at the bottom of the alumina container.

**Crystal Structure of $Ce_2CoGa_9Ge_2$.** The structure of $Ce_2CoGa_9Ge_2$ projected onto *ac*-plane is depicted in Figure 1A. The Co, Ga, and Ge form a three-dimensional $[CoGa_9Ge_2]$ framework, where Ce atoms are filling the voids, forming a monatomic square net (*I*). The $[CoGa_9Ge_2]$ substructure could be further "broken down" to a pair of 2D fragments, namely a $[CoGa_4Ge_2]$ "cube" layer (*II*) and a Ga-only "pentagonal" slab (*III*). The $[CoGa_4Ge_2]$ layer is a common structural feature among ternary rare-earth nickel polygallides like $Ce_2NiGa_{10}$,[40] $Pr_3NiGa_{10}$,[41] $Ce_4NiGa_{18}$,[42] $Sm_2NiGa_{12}$[23] and quaternary rare-earth transitional metal trielides tetrelides such as $REMGa_3Ge$[24] and $RE_3Ni_3Ga_8Ge_3$,[20] $Sm_2Ni(Ni_xSi_{1-x})Al_4Si_6$, and $Ce_2NiAl_{6-x}Ge_{4-y}$.[39] In this layer, the Ga(1) atoms form a distorted cubic arrangement. In $Ce_2CoGa_9Ge_2$ the distortion is severe, with the Ga(1)−Ga(1) distances ranging from 2.562(2) Å to 3.102(2) Å, and it is even more pronounced than in the flat square net of Ga atoms found in $GdCoGa_3Ge$[21] and $YCoGa_3Ge$, where Ga−Ga distances vary within the cubes from 2.615(3) Å to 2.9615(5) Å.[20] Considering such a large divergence in the Ga−Ga bonding in the Ga(1) "cube" layer, it is perhaps more appropriate to view the latter as a set of $[Ga(1)_2]$ dimers, (Ga−Ga = 2.562(2) Å). The Co atoms occupy centers of a half of $[Ga(1)_8]$ "cubes" in a checkered manner, while the remaining half is bicapped with Ge atoms. The distance from the central Co atom to the corners of Ga "cubes" is 2.4655(6) Å, comparable to that found in $YCoGa_3Ge$ (Co−Ga = 2.462(1)

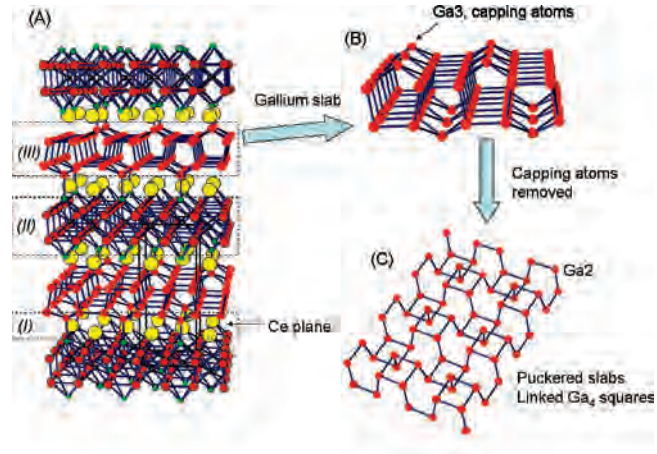


**Figure 1.** (A) Crystal structure of $Ce_2CoGa_9Ge_2$ viewed along the *c*-axis. The Ce, Co, Ga, and Ge atoms are shown with yellow, black, red, and green spheres, respectively. The bonds to Ce atoms are omitted for clarity; the unit cell is shown with a black solid line. Three main structural fragments are contoured with dashed lines and marked with letters (I), (II) and (III) indicating Ce, $[CoGa_4Ge_2]$, and $[Ga(2)_4Ga(3)]$ slabs, respectively. (B) An excised portion of a $[Ga(2)_4Ga(3)]$ "pentagonal" slab. (C) A Ga(2) puckered layer formed by two tetragonal Ga(2) sheets arranged in a staggered conformation and linked across at 2.508(2) Å.

(39) Sieve, B.; Trikalitis, P. N.; Kanatzidis, M. G. *Z. Anorg. Allg. Chem.* **2002**, *628* (7), 1568–1574.

Å).[20] The capping Ge(1) and Ge(2) atoms are bonded to the Ga(1) network at 2.6743(18) Å and 2.772(2) Å.

The Ga-only two-dimensional (2D) network [$Ga(2)_4Ga(3)$] features pentagonal tunnels which run parallel to the *a*-, *b*-axis, see Figure 1A. It could be viewed as consisting of two corrugated 2D Ga sheets (Figure 1B), where the Ga atoms are arranged with a tetragonal symmetry. The Ga−Ga contacts within the [$Ga(2)_4$] squares are 2.5482(18) Å and are strongly bonding, whereas the distance between the squares exceeds 3.4 Å and is nonbonding. A half of the larger hollows of the Ga(2) square net is monocapped with Ga(3) atoms at 2.6075(16) Å. The two corrugated Ga sheets are arranged in a staggered conformation to each other and bonded across via Ga(2)−Ga(2) interactions at 2.508(2) Å, see Figure 1C. This Ga(2)−Ga(2) interaction is the shortest Ga−Ga distance found in this structure. The [$CoGa_4Ge_2$] and Ga-only fragments alternate along the *c*-axis and bridged through the Ge(1) atoms. The Ce atoms form a square pattern with interatomic distances of 4.213 Å. This Ce−Ce interaction is quite typical and has been observed in a number of Ce-containing intermetallic compounds.[43−45] The next closest Ce−Ce interaction occurs at 5.9582(5) Å (unit cell parameter *a*).

The local coordination of all atoms is shown in Figure 2. The Ga(1) atoms are seven-coordinate; they are bonded to six atoms [$Ga(1)_3Ge(2)Co_2$] in the form of a hexagon in the chair conformation and to an additional Ge(1) atom in the apex position. The distances from the central Ga(1) atom to the Ga(1) atoms of the hexagon are 2.562(2) Å and 2.8566(17) Å and to the Ge(2) and Co atoms are 2.772(2) Å and 2.4655(6)Å, respectively. The immediate environment of Ga(2) includes three Ga(2) atoms at 2.508(2) Å and 2.5482(18) Å and one Ga(3) at 2.6075(16) Å in the shape of a severely distorted tetrahedron (Ga(2)−Ga(2)−Ga(2) and Ga(2)−Ga(2)−Ga(3) angles are 90°−99.89(4)°) and 130.83-(2)°−98.31(9)°, respectively). The Ga(3) atoms are located in the center of the square pyramid with the base of four Ga(2) atoms and an apex of Ge(1) atom (Ga(3)−Ge(1) = 2.490(3) Å; the Ge(1)−Ga(3)−Ga(2) angle is 112.37(6)°. Analogously, Ge(1) has a square pyramidal environment that includes four Ga(1) atoms at the pyramid base (Ge(1)−Ga(1) = 2.67443(18) Å) and a Ga(3) atom in the apex position. The Ga(3)−Ge(1)−Ga(1) angle is 124.91(5)°. The Ge(2) atoms are four-coordinate; they are bonded equidistantly to four Ga(1) atoms with Ge(2)−Ga(1)−Ga(1) bond angle of 58.98(2)°. The Co atoms are in the center of the distorted cube of eight Ga(1) atoms; the Co−Ga(1) bond is 2.4655(6) Å, and the Ga(1)−Co−Ga(1) bond angles are 62.61(4)° 70.81(5)°, 77.95(5)°, 105.59(2)°, 117.55(4), and 175.97(6)°.

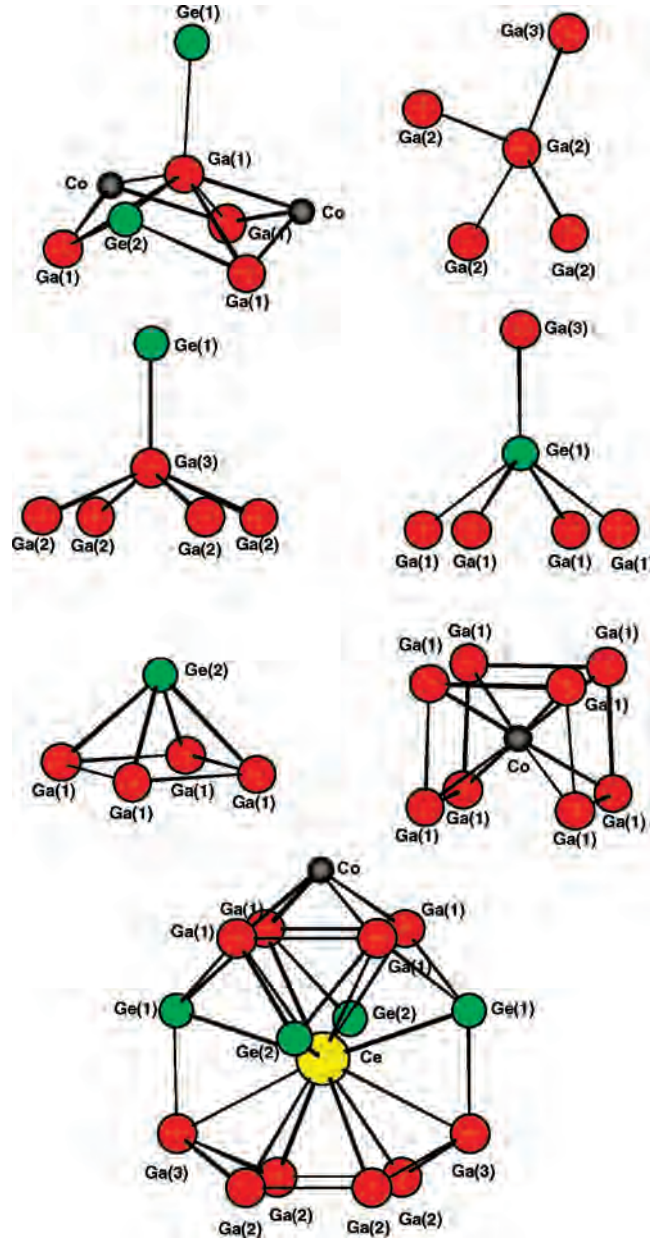


**Figure 2.** Local coordination environments of Ga, Ge, and Co atoms (shown within the sphere of radius 3.0 Å) and Ce atoms (within 3.5 Å).

The 14-atom coordination polyhedron of the Ce atoms includes ten Ga atoms (Ce−Ga(1) = 3.2843(11) Å; Ce−Ga(2) = 3.2789(11) Å; Ce−Ga(3) = 3.3362(12) Å) and four Ge atoms (Ce−Ge(1) = 3.1387(8) Å; Ce−Ge(2) = 3.0430(6) Å). For a more complete list of bond distances and bond angles see the Supporting Information.

Although $Ce_2CoGa_9Ge_2$ is a Ga-rich compound, the Ga atoms do not form an extended network on their own. A Ga-only substructural unit bears zero- and 2D character: Ga(1) atoms form dimers (severely distorted Ga cubes), while Ga(2) and Ga(3) form 2D layers with pentagonal channels. The average Ga−Ga bond distance (for all interactions up to 3.0 Å) is 2.641 Å, which is comparable to the sum of single-bonded metallic radii[46] (2.50 Å) and is quite shorter than the average Ga−Ga distance found in metallic Ga (2.70 Å). The bonding within the Ga framework is thus reasonably strong. Similar Ga−Ga bonding interactions were observed

(40) Yarmolyuk, Y. P.; Grin, Y. N.; Rozhdestvenskaya, I. V.; Usov, O. A.; Kuzmin, A. M.; Bruskov, V. A.; Gladyshevsky, E. I. *Kristallografiya* **1982**, *27* (5), 999–1001.
(41) Grin, Y. N.; Yarmolyuk, Y. P.; Rozhdestvenskaya, I. V. *Kristallografiya* **1983**, *28* (4), 806–808.
(42) Grin, Y. N.; Yarmolyuk, Y. P.; Usov, O. A.; Kuzmin, A. M.; Bruskov, V. A. *Kristallografiya* **1983**, *28* (6), 1207–1209.
(43) Galadzhun, Y. V.; Pottgen, R. *Z. Anorg. Allg. Chem.* **1999**, *625* (3), 481–487.
(44) Niepmann, D.; Pottgen, R.; Kunnen, B.; Kotzyba, G.; Mosel, B. D. *Chem. Mater.* **2000**, *12* (2), 533–539.
(45) Niepmann, D.; Pottgen, R.; Kunnen, B.; Kotzyba, G.; Rosenhahn, C.; Mosel, B. D. *Chem. Mater.* **1999**, *11* (6), 1597–1602.

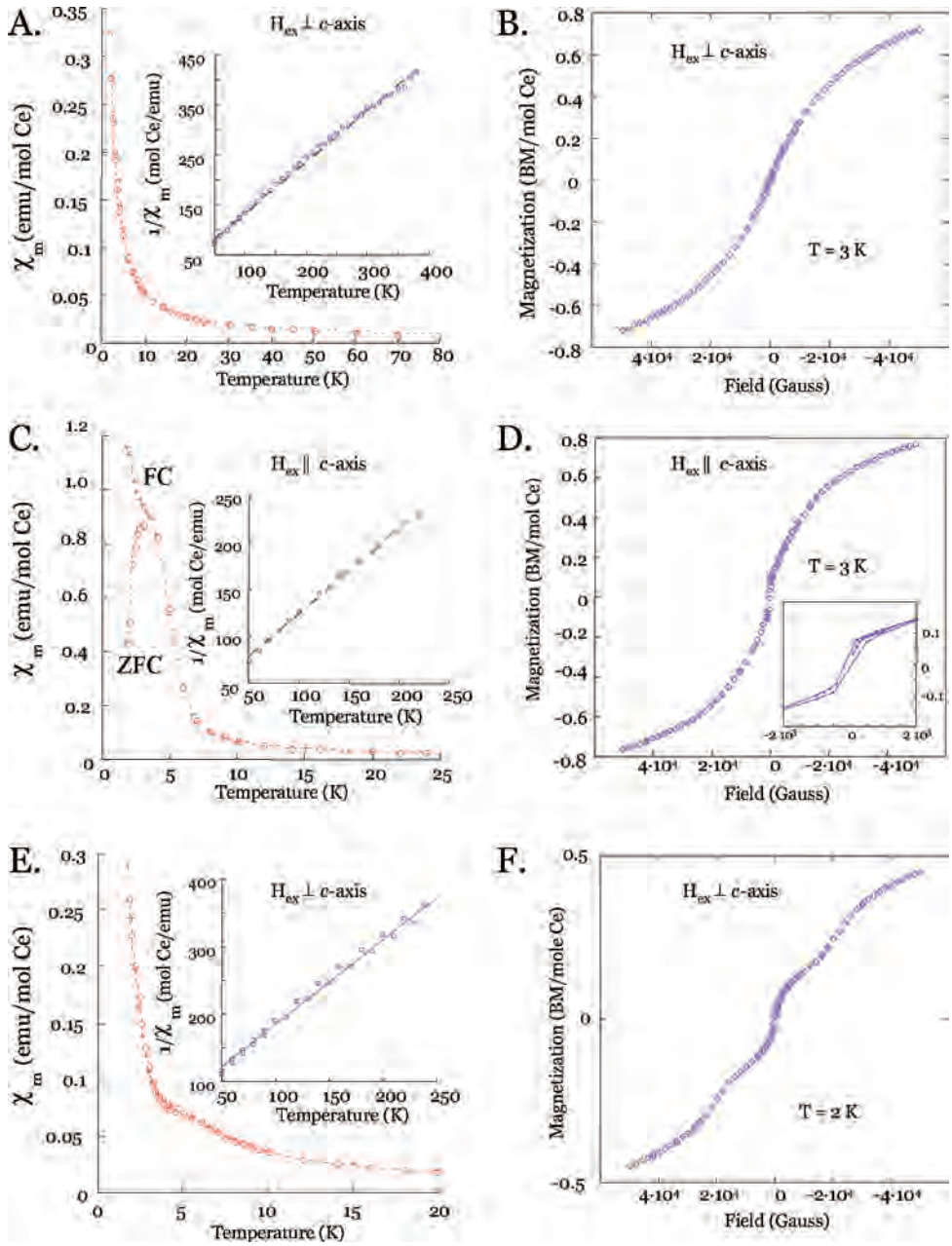


**Figure 3.** (A) Temperature dependence of molar magnetic susceptibility ($\chi^{\perp}_m$) and inverse susceptibility ($(\chi^{\perp}_m)^{-1}$) of $Ce_2NiGa_9Ge_2$ single crystal oriented with the *c*-axis perpendicular to the external magnetic field ($H_{ex}$); inset: linear part of the molar magnetic susceptibility plotted in the 50−400 K temperature range; (B) field dependence of the magnetization of a single crystal of $Ce_2NiGa_9Ge_2$ oriented with *c*-axis perpendicular to $H_{ex}$ measured in fields up to ±5 T at 3 K. (C) Temperature dependence of $\chi^{\parallel}_m$ and $(\chi^{\parallel}_m)^{-1}$ of a $Ce_2NiGa_9Ge_2$ single crystal oriented with the *c*-axis parallel to the external magnetic field; inset: linear part of the molar magnetic susceptibility plotted in the temperature range 50−250 K; (D) field dependence of the magnetization of a single crystal of $Ce_2NiGa_9Ge_2$ oriented with the *c*-axis parallel to $H_{ex}$ in fields up to ±5 T measured at 3 K. Inset: an expanded region of low-field magnetization data (±0.2 T). (E) Temperature dependence of $\chi^{\perp}_m$ and $(\chi^{\perp}_m)^{-1}$ of a $Ce_2CoGa_9Ge_2$ single crystal oriented with the *c*-axis perpendicular to the external magnetic field; inset: linear part of the molar magnetic susceptibility plotted in the temperature range 50−250 K; (F) field dependence of the magnetization of a single crystal of $Ce_2CoGa_9Ge_2$ oriented with the *c*-axis perpendicular to $H_{ex}$ measured in fields up to ± 5 T at 2 K.

in the $Ce_3Ga_9Ge$ polygallide with an average distance of 2.64 Å. The connection between 1D and 2D fragments within the Ga-only network occurs via bridging Ge(1) atoms that link Ga(1) to Ge(1) at 2.6743(18) Å and Ge(1) to Ga(3) at 2.490(3) Å. The latter is the shortest bonding contact in the structure and, in view of the sum of covalent radii of Ga and Ge (2.47 Å), reflects considerable covalent character.

The Ce−Ga interactions cover the range from 3.2789(11) Å to 3.3362(12) Å with an average Ce−Ga bond distance of 3.293 Å. Allowing for the sum of single-bonded metallic radii of Ga (1.25 Å) and Ce (1.818 Å for CN = 12), these interactions could be regarded moderately to weakly bonding. The Ce−Ga bond distances found in $Ce_2CoGa_9Ge_2$ fall in the same range as those found in other Ce-containing gallides such as $Ce_3Ga_9Ge$[24] (3.1139(16) Å−3.4342(9) Å) and $CeRu_2Ga_8$[47] (3.135 Å−3.387 Å).

**Magnetic Properties. (a) $Ce_2NiGa_9Ge_2$.** The temperature-dependent magnetic susceptibility of $Ce_2NiGa_9Ge_2$ was measured anisotropically by positioning a single crystal with the crystallographic *c*-axis parallel ($\chi^{\parallel}_m$) and perpendicular

($\chi^{\perp}_m$) to the external magnetic field ($H_{ex}$). The $\chi^{\perp}_m$ is inversely proportional to $T$ in the whole region of measured temperatures (1.8−400 K) with no upturn in zero-field-cooled−field-cooled (ZFC-FC) history dependence observed up to 1.8 K, see Figure 3A. The inverse molar susceptibility in the high temperature region (50−400 K) could be fitted within the Curie−Weiss law with the effective magnetic moment ($\mu_{eff}$) of 2.80 Bohr magnetons (BM) and the Weiss constant ($\theta$) of −33 K (Figure 3A, inset). The obtained $\mu_{eff}$ is in a good agreement with the theoretical value (2.54 $\mu_B$) given by the formula $\mu_{eff} = g_J[J(J+1)]^{1/2}$, where $g_J$ is a Landé factor,[48] and $J$ is a total angular momentum of the $Ce^{3+}$ ion.[49] The field dependence of magnetization measured in the fields up to ±5 T and calculated in BM per mole of Ce is given in Figure 3B. The onset of saturation of the magnetic moments is observed at 5 T with the total moment of ∼0.8 $\mu_B$. The lowered value of $\mu^{sat}$ compared to the theoretical value (2.14 $\mu_B$), that could be obtained using the formula $\mu^{sat} = g_J$, is indicative of the lifted degeneracy of the $J = 5/2$ ground multiplet of $Ce^{3+}$ ion because of the crystal field.[50−52] Similar experimental values of $\mu^{sat}$ (0.8−1.2) have been previously observed in a number of Ce-containing intermetallic compounds.[53,54]

When the external magnetic field is directed parallel to the $c$-axis, the magnetic response is nearly four times greater than that in perpendicular direction (1.2 emu/mol for $\chi^{||}_m$ compared to 0.33 emu/mol for $\chi^{\perp}_m$), see Figure 3C. A transition to an antiferromagnetic state is observed at ∼4 K. Below the critical temperature ($T_N$), the zero-field-cooled part of $\chi^{||}_m$ rapidly decreases, whereas its field-cooled part continues to rise. Above the $T_N$, the system behaves as a regular paramagnet, as evident from the linear part of $(\chi^{||}_m)^{-1}$ versus $T$ (Figure 3C, inset). The calculation of $\mu_{eff}$ from the high-temperature data of $(\chi^{||}_m)^{-1}$ versus $T$ yields 2.97 $\mu_B$. The Weiss constant is negative, $\theta = -37$ K. The field dependence of magnetization for $H_{ex}||c$ is shown in Figure 3D. Similarly to $H_{ex}\perp c$, the magnetization is practically saturated at 5 T, yielding the value of only 0.8 $\mu_B$ A weak hysteresis loop was observed in the $M(H)$ characterized with a very small remnant magnetization, see Figure 3D (inset).

**(b) $Ce_2CoGa_9Ge_2$.** The susceptibility data for the Co analog is similar to that found for $Ce_2NiGa_9Ge_2$. For example in $Ce_2CoGa_9Ge_2$, the maximal magnetic response at 1.8 K ($\chi^{\perp}_m$ = 0.30 emu/mol) is very close to that observed for $Ce_2NiGa_9Ge_2$ ($\chi^{\perp}_m$ = 0.33 emu/mol), see Figure 3 E. The low temperature area of the $\chi^{\perp}_m - T$ plot shows a broad shoulder centered ∼4 K. The temperature dependence of $(\chi^{\perp}_m)^{-1}$ above 50 K is linear (Figure 3E, inset), obeying the Curie−Weiss law. The experimental $\mu_{eff}$ = 2.53 $\mu_B$ is in excellent agreement with the theoretical value of 2.54 $\mu_B$. The Weiss constant has even larger negative value than in case of $Ce_2NiGa_9Ge_2$, $\theta = -47$ K. The field dependence of the magnetization $M(H)$ for the perpendicular orientation is depicted in Figure 3 F. Here, a maximal moment developed in a field of 5 T is only 0.5 $\mu_B$, less than 25% of the full saturation value. No history dependence was observed for $M(H)$ in the perpendicular orientation.

The magnetocrystalline anisotropy effects studied in $Ce_2NiGa_9Ge_2$ shows the direction of the magnetically easy axis to be along the crystallographic $c$-axis. The perpendicular direction containing basal plane is magnetically hard. Because ordering of magnetic moments in these compounds occurs at quite low temperatures, the direction of the magnetic field with respect to the easy axis of the crystal may obstruct the detection of the magnetic phase transitions or even bring about the effect of their "appearance" and "vanishing".

## Concluding Remarks

Molten gallium has demonstrated the ability to serve both as a reactive and nonreactive solvent in preparation and crystallization of complex intermetallics RE/M/Ga/Ge(Si). There are significant differences in the reaction chemistry of the systems involving Si versus Ge. For instance, Ga-free products are the common outcome of the reactions conducted in the RE/M/Ga/Si system, such as $RENiSi_3$, $RE_2Ni_{3+x}Si_{5-x}$, and $RE_5Co_4Si_{14}$. Contrarily, Ga reactivity is greatly increased in the corresponding Ge-containing reactions. At RE/M < 1, we observe a formation of two very stable hexagonal phases $RE_{0.67}M_2Ga_{5-x+n}Ge_x$ ($n$ = 0, 1) that occur for every rare-earth metal except for Ce, Eu, and Lu. For RE/M ≥ 1, however, the reaction products depend more strongly on the identity of the RE and the reaction conditions. Previously, we have uncovered three families of quaternary phases that form at RE/M ≥ 1: $REMGa_3Ge$, $RE_3M_3Ga_8Ge_3$, and $RE_4M_3Ga_6Ge_4$. The discovery of a new family, $RE_2MGa_9Ge_2$, that forms at RE/M ≥ 1 under Ga flux conditions with RE = Ce and Sm underscores a surprising wealth of intermetallic chemistry that is accessible via flux chemistry.

**Acknowledgment.** Financial support from the Department of Energy (DE-FG02-07ER46356) is gratefully acknowledged.

**Supporting Information Available:** Details of data collection and refinement, tables of crystallographic data, and related information for $Ce_2CoGa_9Ge_2$, and $Sm_2NiGa_9Ge_2$. This material is available free of charge via the Internet at http://pubs.acs.org.

IC801067G

(46) Pauling, L. *The Nature of Chemical Bond and the Structures of Molecules and Solids.*; Cornell University Press: Ithaca, NY, 1960.
(47) Schluter, M.; Jeitschko, W. *Inorg. Chem.* **2001**, *40* (25), 6362–6368.
(48) For the systems with strong spin-orbit coupling the gyromagnetic ratio $g_J = 1 + \{[S(S+1) - L(L+1) + J(J+1)]/[2J(J+1)]\}$, where $S$ is spin momentum, $L$ is orbital momentum, and $J$ is total angular momentum.
(49) The total angular momentum ($J$) of the ion with an unfilled 4f shell is determined by the Hund's rules. $J = L + S$,, $L - S$ for shells greater or less than half full, respectively.
(50) Adroja, D. T.; Rainford, B. D. *Physica B* **1994**, *194*, 363–364.
(51) Rainford, B. D.; Adroja, D. T. *Physica B* **1994**, *194*, 365–366.
(52) Sugawara, T.; Eguchi, H. *J. Phys. Soc. Jpn.* **1966**, *21* (4), 725.
(53) Jones, C. D. W.; Gordon, R. A.; DiSalvo, F. J.; Pottgen, R.; Kremer, R. K. *J. Alloys Compd.* **1997**, *260* (1−2), 50–55.
(54) Pottgen, R.; Borrmann, H.; Kremer, R. K. *J. Magn. Magn. Mater.* **1996**, *152* (1−2), 196–200.